



ENGINEERING SCIENCES

Temperature pull-down of a retrofitted wine refrigerator cabinet cooled by a caloric system emulator

RICARDO S. CALOMENO, SERGIO L. DUTRA, NATÁLIA M. DE SÁ,
GUILHERME F. PEIXER, JAIME A. LOZANO & JADER R. BARBOSA JR.

Abstract: The present study analyzes the time-dependent thermal behavior of a retrofitted wine refrigerator cabinet operated by a caloric system emulator. The presence of a full load of wine bottles enabled the assessment of the thermal stratification inside the cabinet. Further experimental tests have been performed to quantify the overall thermal conductance of the cabinet walls and the thermal conductance of the glass door. A detailed mathematical model was developed to predict the temperature pull down in the refrigerated compartment, considering the interaction between the cabinet air and the wine bottles. In addition to the air and bottle temperatures, a good agreement (lower than 15 % relative error) was observed for the cooling capacity. The numerical simulations revealed that the cabinet door was responsible for approximately 60 % of the thermal load (even though it corresponded to approximately 20 % of the cabinet external area).

Keywords: Caloric cooling, heat exchangers, mathematical modeling, refrigerator cabinet, wine cooler.

INTRODUCTION

Caloric cooling and heat pumping have been the subject of intense research in the past few years (Greco et al. 2019). Of all caloric effects, the magnetocaloric effect – which results from the application of a magnetic field change on a magnetic material to produce a cooling effect (Fähler & Pecharsky 2018, Trevizoli & Barbosa 2020) – is the most studied solid-state phase change phenomenon in the context of the development of refrigerants and lab demonstrators which could evolve, in the near future, into devices capable of functioning in relevant and operational environments (Jacobs et al. 2014, Hirano et al. 2014, Eriksen et al. 2015, Aprea et al. 2016, Dall’Olio et al. 2018, Nakashima et al. 2021, Lionte et al. 2021). Nevertheless, very few studies on magnetic refrigeration have addressed specifically the thermal design of heat exchangers (which are characterized by single-phase heat transfer in both streams) and the effect of cabinet thermal insulation. In fact, most theoretical studies to this date assumed ideal (i.e., infinite thermal conductance) heat exchangers, and most lab demonstrators used Joule effect heaters to emulate the thermal load (Yu et al. 2010, Greco et al. 2019).

Engelbrecht (2004) used the ϵ -NTU method to numerically evaluate the influence of prescribed overall thermal conductances for the hot and cold heat exchangers on the performance of a 150-W domestic freezer driven by a magnetic refrigerator. Chaudron et al. (2014) noted that the cooling capacity and temperature span of an AMR system can be quite sensitive to the effectiveness of the heat

exchangers, which should be designed to have the lowest possible pressure drops (pumping power) and internal volumes. Hittinger et al. (2016) focused on modifying the cold heat exchanger design to make it more compact than the baseline and, by considering the interaction with the fan, obtained lower cabinet air temperatures and higher cooling rates in a 350-Liter refrigerated cabinet. More recently, with a different application in mind (a 2600-W heating capacity residential magnetocaloric heat pump), Johra et al. (2019) used the ϵ -NTU method to design the hydronic under-floor heating system (a horizontal heat exchanger embedded in a multilayer slab) and the vertical borehole ground source heat exchanger.

Although a systematic assessment of refrigerated cabinets for caloric cooling systems is still lacking in the literature, one expects that the basic design and evaluation procedures will follow those normally adopted for conventional cooling technologies. To date, several models have been proposed to describe the steady-state (Gonçalves et al. 2009, Hermes et al. 2009, Tagliafico et al. 2012, Zsembinszki et al. 2017) and dynamic behavior of household refrigerators using quasi-steady and fully transient approaches (Chen & Lin 1991, Janssen et al. 1992, Hermes & Melo 2008, Borges et al. 2011, 2015, Martinez-Ballester et al. 2012, Mastrullo et al. 2014, Heimele et al. 2016). In the case of a wine cooler, the presence of a glass door should require a different treatment for the overall thermal conductance of the cabinet insulation if the thermal leakage through the former needs to be quantified separately.

In the context of caloric technologies, the biggest advantage of developing wine cooler prototypes compared to other applications in the same cooling capacity range (e.g., refrigerators and freezers) is the relatively small temperature span, normally lower than 30°C. The most widely publicized project of this kind was the magnetic refrigeration wine cooler presented by three partner companies in 2015 (Cooling Post 2015). Although some data on typical operating parameters (temperatures and pull-down time) have been disclosed (Rogge 2015), no further details related to the AMR-magnet assembly, fluid management system, heat exchangers and cabinet have been made available in the literature. More recently, Tomc et al. (2018) reported on the development of an AMR wine cooler driven by a 1-T electromagnet system using 100–300 μm Gd spheres. The maximum temperature span achieved was 13 K, for a frequency of 2 Hz.

The present study is part of a research project aimed at developing a domestic wine cooler refrigerated by a compact magnetic system with an electric energy consumption similar to that of a conventional wine cooler, capable of cooling up to 31 wine bottles between 5 and 20°C for an ambient temperature of 25°C. While other papers related to this project have focused on (i) designing the magnet-regenerator assembly for an optimal cooling capacity or coefficient of performance (Fortkamp et al. 2020), (ii) optimizing the heat exchangers for the magnetic wine cooler (Peixer et al. 2022) and (iii) discussing the overall thermodynamic performance of the prototype and proposing potential changes to improve its efficiency (Nakashima et al. 2021), the main objective of the present paper is to advance a mathematical model to analyze the transient heat transfer in the wine refrigerator cabinet. The operating conditions are set by a caloric cooling system emulator (Peixer et al. 2022). The air inside the refrigerated compartment and the emulator interacted via a compact fan-supplied heat exchanger placed inside the cabinet. To validate the mathematical model, temperature pull-down tests were executed (with and without a glass bottle load). Further experimental tests were performed to evaluate the overall thermal conductance of the wine storage cabinet and the overall thermal conductance of the cabinet glass door.

EXPERIMENTAL WORK

Experimental apparatus

The main component of the experimental apparatus is a commercially available 130-Liter wine refrigerator cabinet retrofitted to operate in conjunction with a caloric cooling system emulator (CCSE). The CCSE, described in full by Peixer et al. (2022), consists of two flow loops which independently deliver streams of thermal fluid to the hot and cold heat exchangers at pre-determined temperatures and flow rates. Basic information on the operation of the CCSE are provided below for completeness.

The internal space of the wine refrigerator cabinet was originally divided into two compartments, with a maximum storage capacity of 10 bottles in the upper part and 21 bottles in the lower part, respectively. The cabinet was equipped with an air-filled double-glazed door in which the panes were separated by a 15.5-mm gap. The components of the original vapor compression refrigeration system (expansion devices, compressor, heat exchangers and control system) were removed to allow the cabinet to be connected to the CCSE. However, the maximum storage capacity of the cabinet (31 bottles) remained unchanged.

The dimensions of the wine refrigerator cabinet are shown in Table I. The external liner is made of carbon steel, the thermal insulation is made of cyclopentane-expanded polyurethane (PU) and the internal liner is made of high-impact polystyrene (HIPS). The wine bottles used in the experiments were made of soda-lime glass with external and internal radii of 3.85 and 3.45 cm, an internal volume of 750 cm³ and an equivalent height of 20 cm. The bottles were filled with water. The thermophysical properties of the materials are presented in Table II.

Table I. Cabinet dimensions.

Cabinet width, W	43 cm
Cabinet depth, L	42 cm
Cabinet height, H	83 cm
Wall thickness, L_{wl}	4.23 cm
Internal liner thickness, L_{il}	0.57 cm
Thermal insulation thickness, L_{ti}	3.53 cm
External liner thickness, L_{el}	0.13 cm

Table II. Thermophysical properties of the cabinet walls and wine bottles. For HIPS and glass, the properties were obtained from EES (Klein 2018). For PU and steel, the properties were obtained from Raznjevic (1976).

Material	HIPS	PU	Steel	Glass
ρ , kg m ⁻³	1050	34.5	7850	2440
c_p , J kg ⁻¹ K ⁻¹	1350	1460	477	840
k , W m ⁻¹ K ⁻¹	0.16	0.0214	50	0.937
ϵ_{el}	-	-	0.90	-

The original natural draft roll bond evaporator and wire-on-tube condenser were replaced by fan-assisted wavy fin tube-fin heat exchangers. The new cold heat exchanger was mounted at the top part of the cabinet, as shown schematically in Fig. 1. The hot heat exchanger was placed in the rear bottom part of the cabinet (not visible in the figure).

The cold and hot heat exchangers were connected to independent flow loops in the CCSE. Each flow loop independently controlled the inlet temperature and the mass flow rate of the thermal fluid (a 20% vol. solution of ethylene glycol with corrosion inhibitors in deionized water) into their respective heat exchanger, thus emulating the temperature and thermal capacity rates of the fluid leaving the active caloric regenerator (ACR) during the isofield hot and cold blows, respectively. A picture of the

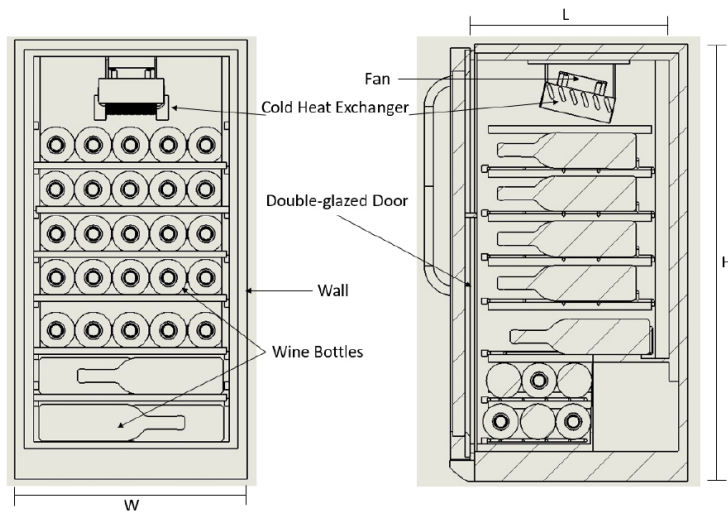


Figure 1. Schematic views (front and side) of the retrofitted wine refrigerator cabinet.

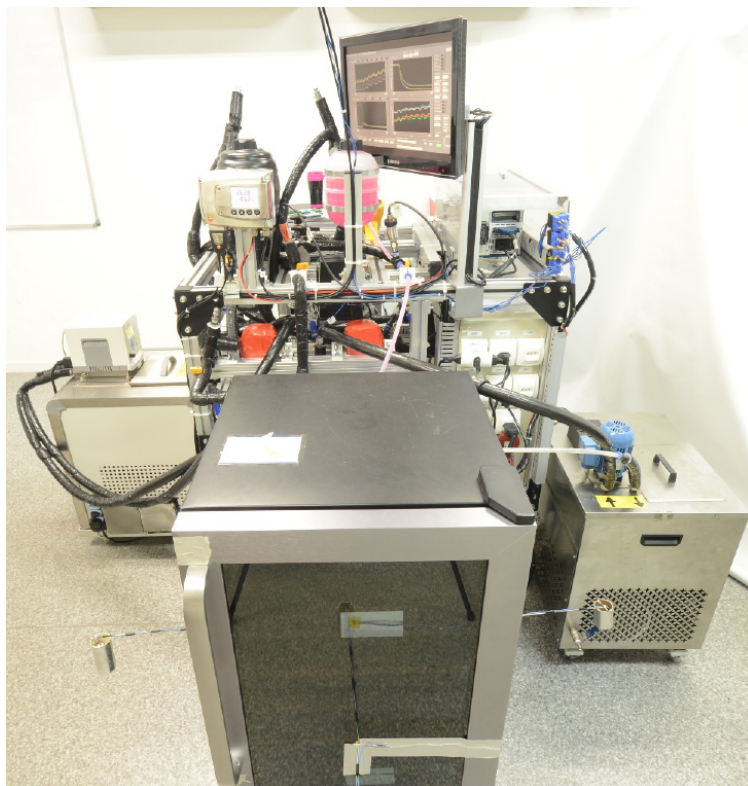


Figure 2. Wine refrigerator cabinet connected to the caloric cooling system emulator (CCSE).

CCSE connected to the wine refrigerator cabinet is shown in Fig. 2. A more detailed description of the design and operation of the CCSE can be found in Peixer et al. (2022).

Experimental tests

Experimental tests were carried out to determine the thermal behavior of the wine refrigerator cabinet operating at steady-state and transient conditions. While the steady-state behavior has been

quantified in detail by Peixer et al. (2022), the present paper focuses on the transient experiments and on using the resulting data to validate a transient thermal model.

The transient behavior of the cabinet was analyzed by means of temperature pull-down tests, which consist of cooling the air inside the refrigerated cabinet from the external environment temperature down to an equilibrium temperature. In the present setup, the time required to reach the equilibrium temperature depends, in principle, of (i) the ambient temperature, (ii) the overall thermal conductance of the cabinet, (iii) the mass flow rate of the thermal fluid through the heat exchangers, (iv) the temperature of the thermal fluid at the inlet of each heat exchanger and (v) the number of wine bottles inside the cabinet. By definition, the equilibrium temperature itself depends on (i)-(iv), but not on (v), as confirmed experimentally by Peixer et al. (2022).

Preliminary tests carried out by Peixer et al. (2022) showed that the liquid mass flow rate in the cold circuit, normally ranging from 40 and 150 kg h⁻¹ in their tests, had little influence on the final temperature of the cabinet. Also, by comparing experiments without a hot heat exchanger and with it in place and operating with a steady flow of thermal fluid with an inlet temperature of 40°C, it was observed that the influence of the latter on the cabinet air temperature was negligible. Therefore, the main independent parameters in the present transient tests were the following:

- *Geometry (number of tube rows) of the cold heat exchanger:* Two herringbone wavy-fin tube-fin heat exchangers with similar characteristics (one with a single tube row and another with two tube rows, namely heat exchangers CHEX #1 and CHEX #2) were tested. The geometric properties of the heat exchangers are presented in the Appendix;
- *Number of wine bottles inside the cabinet:* Only the full-load (31 bottles) and zero-load (0 bottles) conditions were tested, intermediate scenarios were not evaluated;
- *Cold heat exchanger inlet temperature:* The inlet temperature was varied from 273 to 276 K so that the air inside the cabinet could reach equilibrium temperatures of approximately 278 K, according to previous steady-state measurements (Peixer et al. 2022).

The transient tests were carried out at an ambient temperature of 298 ± 1 K and relative humidity between 40% and 70% (maintained by an air conditioner powered by a variable-speed compressor). Each test begins with the cabinet (and the glass bottle load, if applicable) at thermal equilibrium with the external environment. The cold flow loop is started, but the cold fluid is allowed to flow into the cold heat exchanger (to generate a cooling capacity in the cabinet) only after the desired liquid inlet temperature, $T_{f,in}$, is achieved. Then, the cabinet door is closed and the heat exchanger fan is switched on. Data acquisition at a frequency of 1 Hz begins before the cabinet door is closed (to ascertain that the initial thermal equilibrium is verified during post-processing) and continues until steady state is reached. The main output variables of the transient tests are the mean temperatures of the internal air and of the bottles. The mean temperature of the internal air was calculated from an average of 3 thermocouples distributed inside the cabinet, one of them is located in the top region, one in the middle and one at the bottom (Peixer et al. 2022). The mean temperature of the bottles was calculated from an average of 7 bottles placed at various positions inside the cabinet. Thermocouples were positioned inside each bottle to measure the temperature of the water inside. The temperature

pull-down tests ended when the mean air temperature variation was lower than 0.1 K within a 20 minutes period.

MATHEMATICAL MODELLING

Fig. 3 presents a schematic thermal network of the wine cooler cabinet. The three thermal domains of the model are (i) the cabinet walls, (ii) the wine bottles and (iii) the air inside the cabinet. A detailed description of each model and their equations will be given next.

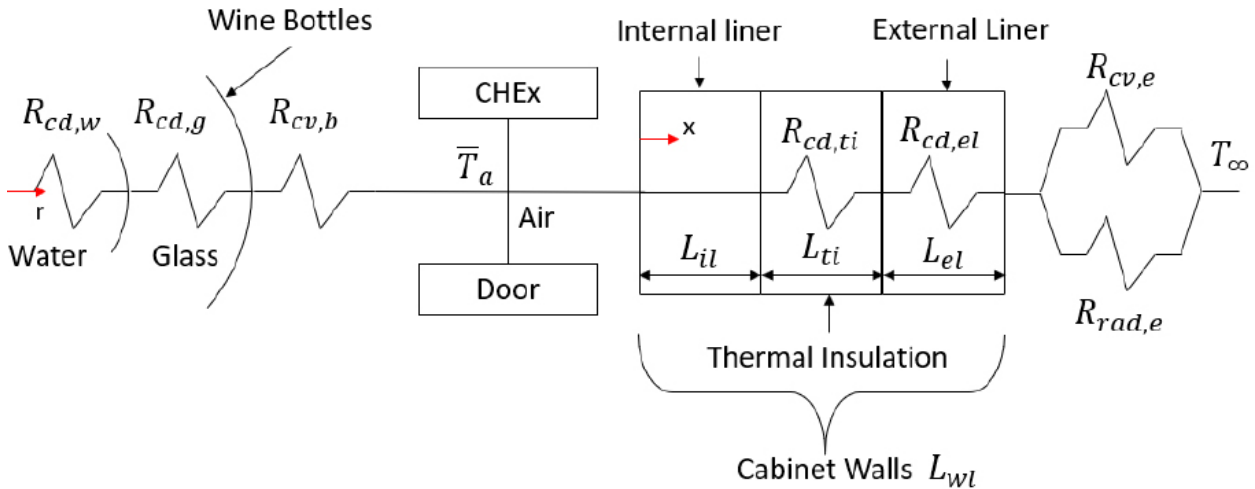


Figure 3. Thermal resistance network connecting the three thermal domains (cabinet walls, wine bottles and internal cabinet air).

Cabinet walls

The cabinet walls were divided into three domains: the external liner, the (intermediate) thermal insulation and the internal liner (which provides structural support to the internal shelves). A scaling analysis revealed that the conduction thermal resistance of the intermediate insulation layer is 10² and 10 times greater than the thermal resistances of the internal liner (conduction) and of the internal natural convection along cabinet walls, respectively. Thus, both resistances (internal liner and internal air convection) were disregarded in the analysis, and the thermal capacity of the internal liner was combined with that of the internal air in the balance equation for the latter (see Section Cabinet air), as proposed by Hermes & Melo (2008). The thermal insulation layer and the external liner were modeled as flat plates in which the heat conduction was assumed one-dimensional along its shortest dimension (thickness) as follows:

$$\rho c_p \frac{\partial T}{\partial t} = \frac{\partial}{\partial x} \left(k \frac{\partial T}{\partial x} \right) \tag{1}$$

where *T* is the temperature along the wall. Although the physical properties are assumed uniform in each domain of the composite cabinet wall, the discontinuity of the thermal conductivity at the interface between two domains is a requirement for it to remain inside the parenthesis in Eq. (1).

The first boundary condition to Eq. (1) is a prescribed temperature at the interface between the internal liner and the thermal insulation, *x* = *L_{il}* (see Fig. 3). Since the internal liner has a negligible

thermal resistance and its thermal capacity has been combined with that of the internal air, it is reasonable to assume that it remains in thermal equilibrium with the air inside the cabinet. At $x = L_{wl} = L_{il} + L_{ti} + L_{el}$, a boundary condition of the third kind is applied combining thermal radiation and natural convection on the outer surface of the external liner in contact with the ambient air:

$$\left(k_{el} \frac{\partial T}{\partial x} \right) \Big|_{x=L_{wl}} = (h_{rad,e} + h_{cv,e})(T_{\infty} - T|_{x=L_{wl}}) \quad (2)$$

The radiation heat transfer coefficient, $h_{rad,e}$, is calculated assuming that the surrounding surfaces are in thermal equilibrium with the ambient air. Thus:

$$h_{rad,e} = \varepsilon_{el} \sigma (T_{\infty}^2 + T|_{x=L_{wl}}^2) (T_{\infty} + T|_{x=L_{wl}}) \quad (3)$$

The natural convection heat transfer coefficient, $h_{cv,e}$, was calculated with the correlation of Churchill & Chu (1975) using the cabinet height as the characteristic length.

Wine bottles

The wine bottle domain is composed of two materials, namely the glass and the liquid content, which is assumed to have the physical properties of water according to the recommendations of the IEC 62552-1 International Standard (International Electronic Commission 2015). The physical properties are assumed to be uniform in each region of the bottle domain.

The bottles were modelled as horizontal cylinders, in which the original internal and external radii were kept fixed and the height was adjusted to preserve the original liquid volume. Heat conduction was assumed one-dimensional in the radial direction in the bottle domain (natural convection in the liquid was neglected):

$$\rho_b c_{p,b} \frac{\partial T_b}{\partial t} = \frac{1}{r} \frac{\partial}{\partial r} \left(k_b r \frac{\partial T_b}{\partial r} \right) \quad (4)$$

where a symmetry boundary condition is assumed at $r = 0$ (bottle center line) and a boundary condition of the third kind is applied at the outer surface of the wine bottles ($r = r_o$):

$$\left(k_g \frac{\partial T_b}{\partial r} \right) \Big|_{r=r_o} = \bar{h}_{cv,b} (T_a - T_b|_{r=r_o}) \quad (5)$$

where T_a is the temperature of the air inside the cabinet. Due to the low values of surface emissivity and small temperature differences involved, radiation heat transfer between the surfaces inside the refrigerated compartment of the cabinet were neglected. The air convection around the bottles was modelled as a flow through an in-line bank of tubes with a mean heat transfer coefficient, $\bar{h}_{cv,b}$, computed using the Grimison correlation (Incropera et al. 2006), which is omitted from this paper for the sake of brevity. For the present geometry, the empirical coefficients of this correlation were calculated as $C_1 = 0.348$, $m = 0.592$ (for air flow through an in-line bank of tubes with 10 or more rows). The coefficient C_2 was calculated as 0.94 according to Kays and Lo (Incropera et al. 2006) for a number of tube rows equal to six. The volumetric air flow rate required to determine the Reynolds number associated with the flow through the tube bank was calculated by matching the fan curve (as supplied by its manufacturer) with the cold heat exchanger air-side pressure drop curve (see Section Cabinet air).

Cabinet air

The cabinet air is modelled using a lumped energy balance in which the mean temperature of the air is assumed spatially uniform, varying only with respect to time. Thus:

$$\left(\rho_a^0 V_a c_{p,a} + \rho_{il} A_{cab,i} L_{il} c_{p,il}\right) \frac{\partial T_a}{\partial t} = \dot{Q}_{wl} + \dot{Q}_d + \dot{Q}_b + \dot{Q}_c + \dot{W}_f \quad (6)$$

where ρ_a^0 is the ambient air density evaluated at the temperature of the external environment, V_a is the internal volume of the cabinet, ρ_{il} is the internal liner density, $A_{cab,i}$ is the area of the liner in contact with the air, L_{il} is the internal liner thickness, $c_{p,a}$ and $c_{p,il}$ are, respectively, the specific heat capacities of the air and the internal liner. The first term on the right side of Eq. (6) is the heat transfer rate through the cabinet walls defined as:

$$\dot{Q}_{wl} = -k_{ti} A_w \left. \frac{\partial T}{\partial x} \right|_{x=L_{il}} \quad (7)$$

where the temperature gradient at the surface of the internal liner in Eq. (7) is evaluated numerically at each time step by solving the system of equations presented in Section Cabinet walls. The second term on the right of Eq. (6) is the heat transfer rate through the glass door, calculated assuming that the thermal capacity of the glass door medium is negligible. Thus:

$$\dot{Q}_d = (UA)_d (T_\infty - T_a) \quad (8)$$

where $(UA)_d$ is the overall thermal conductance of the glass door, which considers heat conduction, convection and radiation in the door media. It can be determined by an indirect method which defines it as the difference between the overall thermal conductance of the cabinet, $(UA)_{cab}$, and of the remaining (structural) walls, $(UA)_{st}$:

$$(UA)_d = (UA)_{cab} - (UA)_{st} \quad (9)$$

In the present wine refrigerator cabinet, $(UA)_{cab}$ was experimentally characterized by the reverse heat loss method (Melo et al. 2000, Sim & Ha 2011). In this method, the power dissipated by electric heaters placed at several positions inside the cabinet of the unplugged refrigerator are used in conjunction with local temperature measurements of the air inside the cabinet to compute the cabinet overall thermal conductance from an energy balance. In the present tests, four independent experiments conducted at an ambient temperature of 294 ± 0.2 K and power dissipation rates ranging from 34 to 57.5 W resulted in average air temperatures ranging from 313.6 to 327.2 K and $(UA)_{cab} = 1.747 \pm 0.056$ W K⁻¹ (Peixer et al. 2022). $(UA)_{st}$, in turn, is numerically calculated by the following relationship:

$$\frac{1}{(UA)_{st}} = \frac{1}{A_{cab,i} h_{cv,i}} + \frac{1}{A_{cab,i} \left(\frac{L_{il}}{k_{il}} + \frac{L_{ti}}{k_{ti}} + \frac{L_{el}}{k_{el}} \right)} + \frac{1}{A_{cab,e} (h_{cv,e} + h_{rad,e})} \quad (10)$$

where the first term on the right is the thermal resistance due to natural convection on the internal surface of the cabinet. The second term on the right is the conduction thermal resistance in the composite insulating wall. The third term is the thermal resistance of the combined natural convection and thermal radiation on the external surface of the cabinet. Both the internal and the external convection heat transfer coefficients were evaluated using the Churchill & Chu (1975) correlation.

The radiation heat transfer coefficient was calculated using Eq. (3). By using the data for the four independent measurements described above, the overall thermal conductance of the glass door, $(UA)_{g,d}$, was equal to $1.126 \pm 0.083 \text{ W K}^{-1}$.

In Eq. (6), the third term on the right is the heat transfer rate associated with the bottles as follows:

$$\dot{Q}_b = N_b \bar{h}_{cv,b} A_b \Delta T_{lm} \quad (11)$$

where N_b is the number of wine bottles, ΔT_{lm} is the log-mean temperature difference between the air and the wine bottles evaluated by the following equation:

$$\Delta T_{lm} = \frac{(T|_{r=r_o} - T_{a,out}) - (T|_{r=r_o} - T_{b,out})}{\ln\left(\frac{T|_{r=r_o} - T_{a,out}}{T|_{r=r_o} - T_{b,out}}\right)} \quad (12)$$

where $T_{a,out}$ is the temperature of the air leaving the cold heat exchanger and $T_{b,out}$ is the temperature of the air after passing through all wine bottles, which is given by the following equation:

$$T_{b,out} = T|_{r=r_o} - (T|_{r=r_o} - T_{a,out}) \exp\left(-\frac{\pi D N_b \bar{h}_{cv,b}}{\rho_a \bar{u} N_t S_t C_{p,a}}\right) \quad (13)$$

where N_t is the number of bottles in the transverse (horizontal) direction (see Fig. 1).

The cooling capacity, i.e, the fourth term on the right side of Eq. (6) is calculated assuming that the cold heat exchanger has a negligible thermal capacity. Thus:

$$\dot{Q}_c = \epsilon \dot{C}_{min} (T_{a,in} - T_{f,in}) \quad (14)$$

where $\epsilon = \epsilon(\text{NTU}, C^*)$ is the cold heat exchanger effectiveness evaluated using the ESDU (1991) relationships for cross-flow arrangements of non-mixed streams with one and two tube rows. The number of transfer units, NTU, was calculated assuming that the overall thermal conductance of the cold heat exchanger comprises thermal resistances due to internal forced convection, calculated using the Gnielinski (2013) correlation, tube wall conduction and air-side forced convection in herringbone wavy fin-tube heat exchangers (Wang 2000). In the latter resistance, the overall surface efficiency was computed using the Schmidt approximation (Perrotin & Clodic 2003). In Eq. (14), \dot{C}_{min} is the lowest thermal capacity rate of the two streams, $T_{a,in}$ and $T_{f,in}$ are the inlet temperatures of the air and of the thermal fluid.

The fan power was calculated as follows:

$$\dot{W}_{fan} = \frac{\dot{V}_a \Delta P_a}{\eta_{fan}} \quad (15)$$

where the air-side pressure drop, ΔP_a , was computed taking the acceleration and friction components into account (Shah & Sekulić 2003). In the latter component, the friction factor was calculated using the correlation of Wang (2000) for herringbone wavy fin-tube heat exchangers. The fan efficiency, η_{fan} , was assumed equal to 10 %, since this is a typical value for commercially available refrigerator fans.

The initial condition to Eq. (6) is the temperature of the air inside the cooling compartment at the beginning of the cooling process which is the same as the air of the external environment, thus $T_a(t=0) = T_\infty(t=0)$.

Numerical simulation parameters

The partial differential equations that govern the temperature distributions in the cabinet walls and bottle domains, Eqs. (1) and (4), and their respective boundary conditions, were solved numerically via the finite volume method (Patankar 1980, Versteeg & Malalasekera 2007) using a fully implicit formulation. Equation (6) was solved numerically using the Euler implicit method. The numerical solution was implemented in Python 3.7.3 on the Spyder 3.3.3 platform.

As presented in detail in Section Experimental tests, the following experimental data were used as input to the temperature pull-down simulations: (i) the cold heat exchanger inlet temperature, (ii) the cold heat exchanger thermal fluid mass flow rate, and (iii) the external ambient temperature.

RESULTS

Fig. 4 shows the behavior of the mean cabinet air temperature (model predictions and experimental data) during temperature pull-down tests using CHEx #1 (top figure) and CHEx #2 (bottom figure) in tests without a bottle load, for a thermal fluid inlet temperature of 276.0 K. To give an idea of the thermal stratification in the cabinet, the temperatures measured by the thermocouples in the upper, middle and the bottom regions of the cabinet are displayed as T1, T2 and T3, respectively. The agreement between the model and the experimental data (mean temperature) is within the experimental uncertainty (± 0.3 K). Although the average cabinet air temperature is well predicted by the model, it is slightly under predicted possibly because of some neglected thermal capacity effects, such as those related to the heat exchanger itself and to cabinet shelves/trays (which may be more important at earlier times). As a retrofitted cabinet was used in these experimental tests, some stratification on the air temperature was expected (no prior assessment of the original product has been performed to evaluate the air flow distribution). This stratification can be identified through the individual air temperature traces shown in each figure. Thus, in the test carried out with CHEx #2, whose heat transfer area is larger than that of CHEx #1, these temperature deviations are larger at the beginning of the test, then the air cabinet temperature reaches a uniform stage.

Results for tests performed with a full bottle load for both cold heat exchangers CHEx #1 and CHEx #2 are presented in Fig. 5, which shows the average temperatures of the cabinet air and the wine bottles, together with the model predictions. The thermal fluid inlet temperature is 275.7 K for CHEx #1 and 276.1 K for CHEx #2. As expected, the temperature pull-down time increases significantly in the presence of the wine bottles due to the extra thermal capacity. Fig. 5 also shows the temperatures measured by all air-side thermocouples. During the early stages of the cooling process, a significant stratification of the air cabinet temperature is observed, with higher temperatures inside the bank of bottles and in the bottom region, in comparison to the top region. The presence of the bottles also favors the formation of air flow recirculation regions inside the bottle bank, which reduces the actual heat transfer coefficient around the wine bottles and leads to an overestimation of the temperature decay rate predicted by the model during earlier times. There is a little deviation between the model predictions and the experimental results for the average temperature of the wine bottles which may be due to the temperature of the air after passing through all wine bottles ($T_{b,out}$) being higher than what is actually observed in the experimental tests. This reduces the calculated heat transfer rate

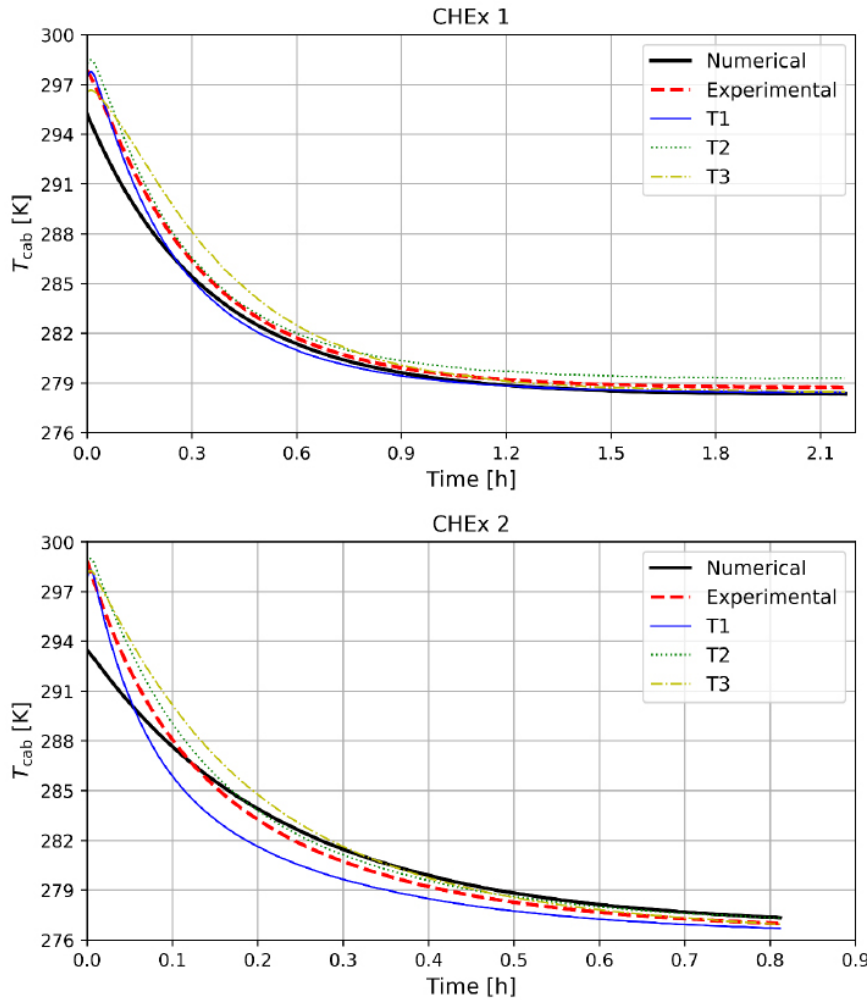


Figure 4. Comparison between the experimental results and model predictions of the mean air temperature inside the cabinet without a bottle load. The thermocouple readings for the top (T1), middle (T2) and bottom (T3) regions are also shown. The temperature of the thermal fluid at the inlet of cold heat exchanger is 276 K for CHEx #1 and CHEx #2.

through the wine bottles. Another potential source of error is the lack of distinction between bottles with regard to the position they occupy inside the cabinet and, consequently, to the effects of position on the temperature difference and thermal conductance for each bottle (see Eq. 11). However, such an effect can only be quantified with a more detailed and computationally expensive mathematical model.

To facilitate the comparison between the temperature pull-down curves obtained with CHEx #1 and CHEx #2, Fig. 6 presents the data in terms of a dimensionless average cabinet air temperature, Θ , and a dimensionless test time, τ , defined as:

$$\Theta = \frac{T_{cab}(\tau) - T_{f,in}(\tau)}{T_{\infty}(\tau) - T_{f,in}(\tau)} \tag{16}$$

and

$$\tau = \frac{t}{t_{td}} \tag{17}$$

where t is time and t_{td} is the test duration.

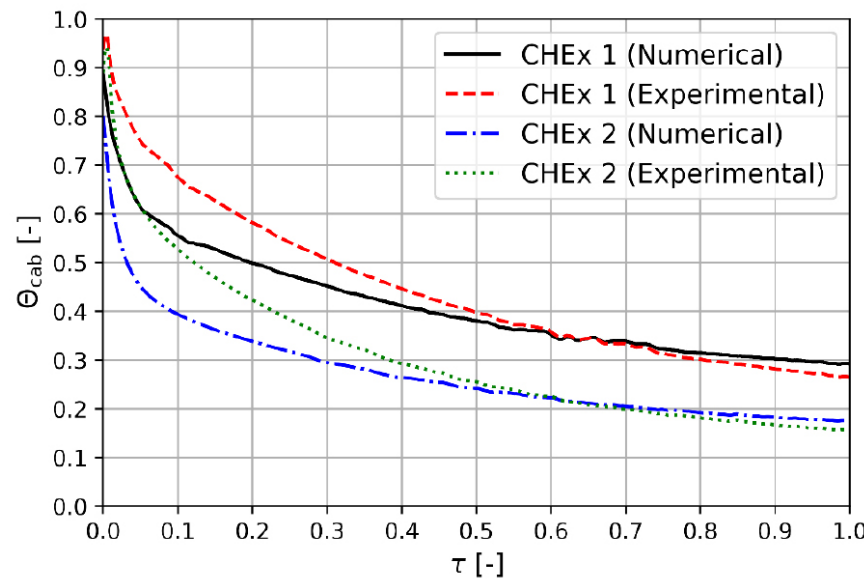
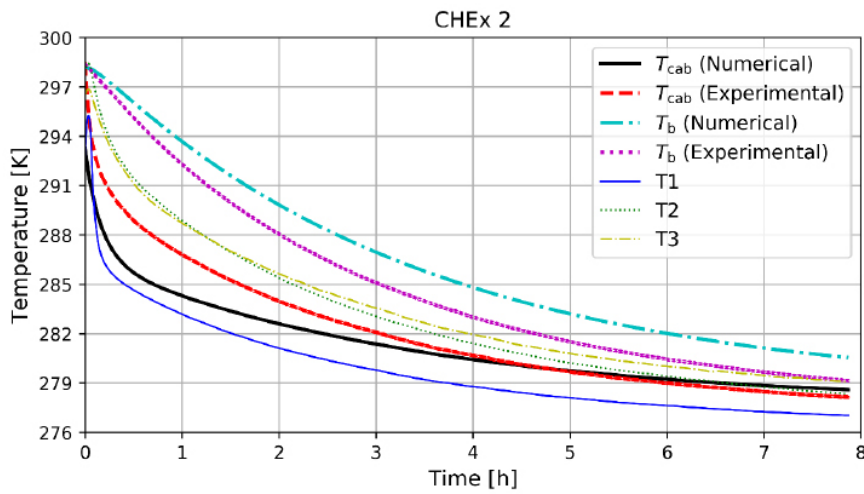
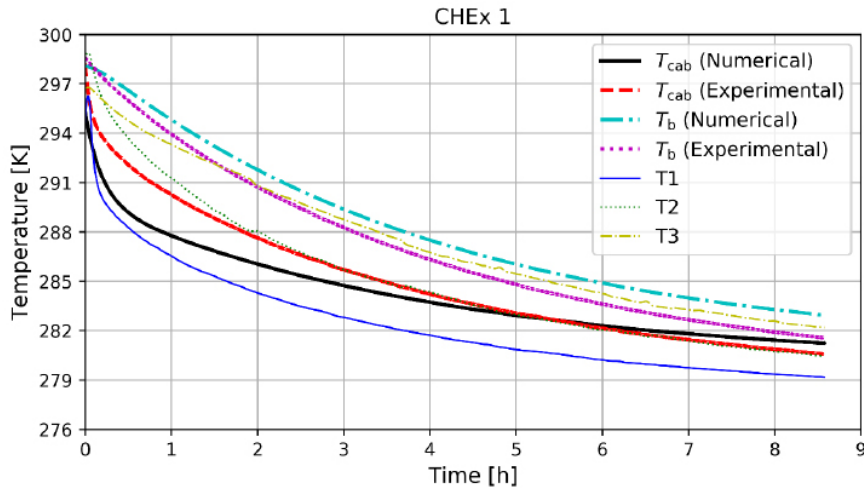


Figure 5. Comparison between the experimental results and model predictions of the mean air temperature inside the cabinet and mean bottle temperature for a full bottle load. The thermocouple readings for the top (T1), middle (T2) and bottom (T3) regions are also shown. The temperature of the thermal fluid at the inlet of cold heat exchanger is 275.6 K for CHEX #1 and 276.1 K for CHEX #2.

Figure 6. Comparison of the dimensionless temperature pull-down curves (mean cabinet air temperature) for tests with a full bottle load.

Fig. 6 clarifies the impact of the overall thermal conductance of the cold heat exchanger on the temperature pull-down. For CHEx #1, the overall thermal conductance was calculated at 10.47 W K^{-1} , while for CHEx #2 it was equal to 20.88 W K^{-1} . Therefore, it becomes clear that when the cabinet is equipped with CHEx #2, the magnetic refrigerator emulator is capable of cooling the air inside the cabinet down to lower temperatures at a fraction of the time required for CHEx #1. During the initial 20% of the pull-down period, a more pronounced stratification of the air temperature inside the cabinet is observed, resulting in higher differences between the experimental data and the numerical results. However, after about 30% of the pull-down period the temperature stratification is reduced leading to a better agreement between the model and the data.

The behavior of the cooling capacity predicted by the model and its comparison with the experimental cooling capacity obtained from an energy balance between the inlet and outlet of the thermal fluid in the cold heat exchanger is presented in Fig. 7, for the same condition of Figs. 5 and 6. As discussed above, the higher values of the cooling capacity predicted by the model can be attributed to the fact that the real air-side heat transfer coefficient may be lower than the actual value due to flow and temperature non-uniformities within the bottle bank. Nevertheless, the agreement improves substantially towards the end of the pull-down time.

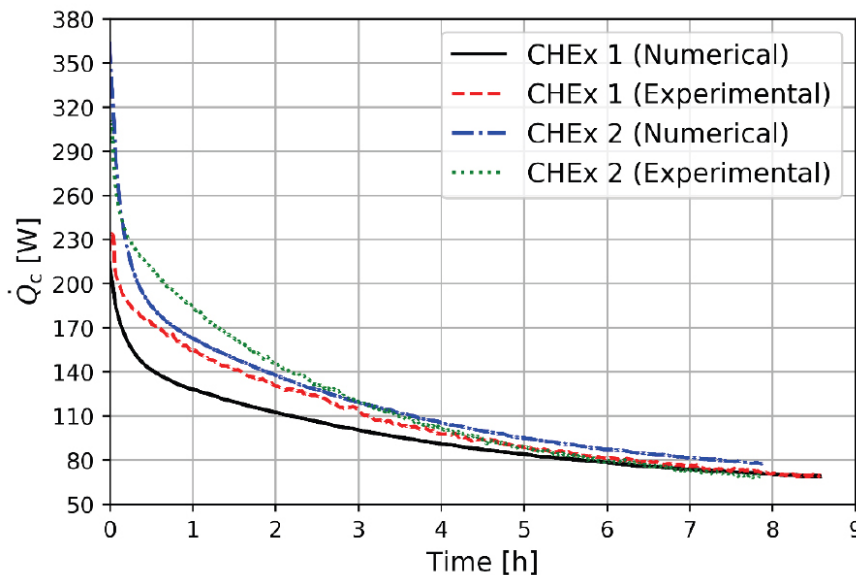


Figure 7. Comparison between the experimental results and model predictions of the cooling capacity in tests with a full bottle load. The temperature of the thermal fluid at the inlet of cold heat exchanger is 275.6 K for CHEx #1 and 276.1 K for CHEx #2.

The individual contributions to the overall thermal load on the cabinet air (wine bottles, cabinet door and cabinet walls) predicted by the model are presented in Fig. 8 for a particular situation in which the wine bottles (and the cabinet air) were initially at the external ambient temperature (298.2 K). The cold heat exchanger fan power consumption is approximately 5 W and is not shown in the figure. In this situation, the highest thermal load generated inside the cabinet is due to the wine bottles being cooled by the air. Considering only the thermal loads from the external environment, the cabinet door is responsible for approximately 6% of this quantity, despite the fact that it covers only around 20% of the external area of the wine refrigerator. Therefore, improving the thermal insulation of the double-glazed door could significantly decrease the total thermal load and reduce the energy

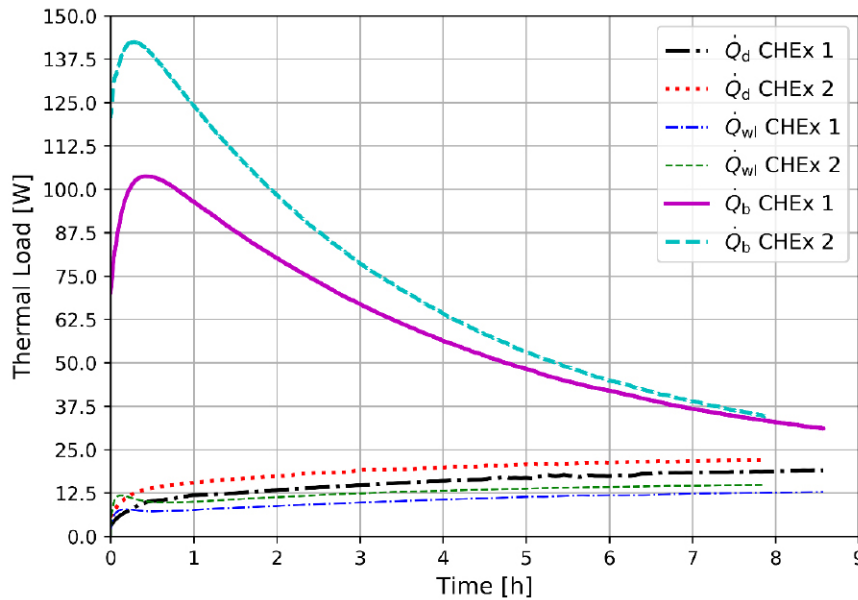


Figure 8. Individual contributions to the thermal load (wine bottles, cabinet door and cabinet walls) predicted by the model for the tests with a full bottle load. The temperature of the thermal fluid at the inlet of cold heat exchanger is 275.6 K for CHEX #1 and 276.1 K for CHEX #2.

consumption. As the steady state is approached and the temperature of the wine bottles becomes close to the that of the air, the cabinet door becomes the main source of thermal load.

CONCLUSIONS

The temperature pull-down behavior of a wine storage cabinet intended for operation with a magnetic refrigeration system was analyzed experimentally and numerically. First, experimental pull-down tests were carried out on the wine storage cabinet with and without a bottle load. The behavior of the thermal fluid received by the cold heat exchanger during the low-field hot blow of magnetic refrigerator was emulated by an experimental apparatus. Then, a mathematical model of the transient heat transfer in the cabinet with a double-glazed door was developed. The overall thermal conductance of the door was determined by an indirect method using experimental data for the reverse heat leakage test and modeling results. Numerical simulations were carried out to evaluate the temporal temperature profile of the air and the wine bottles and the cooling capacity.

The experimental data and the model predictions are in good agreement. In the tests with a full bottle load, the temperature deviations between the experiment and the model at the beginning of the pull-down test were caused mainly by stratification of the air temperature inside the cabinet, which seems to be proportional to the thermal capacity of the bottles. However, after approximately 30% of the pull-down period these variations became smaller and a much better agreement was observed. Also, during the transient period, the major contribution to the thermal load was the cooling of the wine bottles. However, when evaluating only the thermal load associated with the external environment temperature, roughly 60% was through the double-glazed door, which corresponds to 20% of the total external area of the wine refrigerator. This gives a clear indication as to which components should be given priority when optimizing the cabinet insulation.

LIST OF SYMBOLS**Roman**

A	surface area, m ²
\dot{C}	thermal capacity rate, W K ⁻¹
C^*	thermal capacity rate ratio
c_p	isobaric specific heat capacity, J kg ⁻¹ K ⁻¹
g	acceleration of gravity, m s ⁻²
H	height, m
h	convective heat transfer coefficient, W m ⁻² K ⁻¹
k	thermal conductivity, W m ⁻¹ K ⁻¹
L	thickness (or depth), m
\dot{m}_i	mass flow rate, kg s ⁻¹
N_b	number of bottles
N_t	number of bottles in transversal direction
NTU	number of transfer units
\dot{Q}	thermal load, W
\dot{Q}_c	cooling capacity, W
R	thermal resistance, K W ⁻¹
r_o	external bottle radius, m
S_t	transversal bottle pitch, m
T	temperature, K
T_∞	temperature of the external environment, K
t	time, h
t_{td}	test duration, h
\bar{u}	mean velocity, m s ⁻¹
UA	overall thermal conductance, W K ⁻¹
V	volume, m ³
\dot{V}	volumetric flow rate, m ³ s ⁻¹
x	distance, m
W	width, m
\dot{W}_f	fan power, W

Greek

ΔP	pressure drop, Pa
ΔT_{lm}	log-mean temperature difference, K
ϵ	heat exchanger effectiveness
ε	emissivity
η_f	fan efficiency
Θ	dimensionless temperature variation
ρ	Density, kg m ⁻³
σ	Stefan-Boltzmann constant, W m ⁻² m ⁻⁴
τ	dimensionless time

Subscripts

a	air
b	bottles
cab	cabinet
cd	conduction
cv	convection
d	door
e	external surface
el	external liner
ele	electric heater
f	fluid
fan	fan
g	glass
il	internal liner
in	inlet
min	minimum
out	outlet
rad	radiation
st	structure of the cabinet
ti	thermal insulation
w	water
wl	wall

Abbreviations

ACR	active caloric regenerator
CCSE	caloric cooling system emulator
HIPS	high impact polystyrene sheet
PU	polyurethane

Acknowledgments

The primary sources of funding for this work were the CNPq (Conselho Nacional de Desenvolvimento Científico e Tecnológico, Grant no. 404023/2019-3), FAPESC (Fundação de Amparo à Pesquisa e Inovação do Estado de Santa Catarina, Grant no. 2019TRO846), CAPES (Coordenação de Aperfeiçoamento de Pessoal de Nível Superior, Grant No. 88887.194773/2018-00), EMBRAPPII (Empresa Brasileira de Pesquisa e Inovação Industrial) and Nidec Global Appliance Compressores e Soluções em Refrigeração Ltda. (formerly Embraco).

REFERENCES

- APREA C, CARDILLO G, GRECO A, MAIORINO A & MASSELLI C. 2016. A rotary permanent magnet magnetic refrigerator based on AMR cycle. *Appl Therm Eng* 101: 699-703. doi:10.1016/j.applthermaleng.2016.01.097.
- BORGES BN, HERMES CJ, GONÇALVES JM & MELO C. 2011. Transient simulation of household refrigerators: A semi-empirical quasi-steady approach. *Appl Energy* 88(3): 748-754. doi:https://doi.org/10.1016/j.apenergy.2010.09.019.
- BORGES BN, MELO C & HERMES CJ. 2015. Transient simulation of a two-door frost-free refrigerator subjected to periodic door opening and evaporator frosting. *Appl Energy* 147: 386-395. doi:https://doi.org/10.1016/j.apenergy.2015.01.089.
- CHAUDRON JB, ELOUAD L, MULLER C, RISSER M & VASILE C. 2014. Specific design of a heat exchanger for a functional magnetic refrigeration system. In: 6th IIR/IIF International Conference on Magnetic Refrigeration at Room Temperature, Thermag VI, Victoria, Canada, 7-10 September, 2 p.
- CHEN ZJ & LIN WH. 1991. Dynamic simulation and optimal matching of a small-scale refrigeration system. *Int J Refrig* 14(6): 329-335. doi:https://doi.org/10.1016/0140-7007(91)90028-F.
- CHURCHILL SW & CHU HH. 1975. Correlating equations for laminar and turbulent free convection from a vertical plate. *Int J Heat Mass Transf* 18(11): 1323-1329. doi:https://doi.org/10.1016/0017-9310(75)90243-4.
- COOLING POST. 2015. Debut for magnetic refrigeration wine cooler. URL <https://www.coolingpost.com/world-news/debut-for-magnetic-refrigeration-wine-cooler/>.
- DALL'OLIO S, ENGELBRECHT K, ERIKSEN D, CIBIN C & BAHL C. 2018. Design and initial experimental results for a new large-scale AMR heat pump for the residential sector. In: 8th IIR International Conference on Magnetic Refrigeration at Room Temperature, Thermag VIII, Darmstadt, Germany, 16-20 September, 2 p.
- ENGELBRECHT K. 2004. A Numerical Model of an Active Magnetic Regenerator Refrigeration System. M.Sc. thesis. University of Wisconsin-Madison (Unpublished), 177 p.
- ERIKSEN D, ENGELBRECHT K, BAHL C, BJØRK R, NIELSEN K, INSINGA A & PRYDS N. 2015. Design and experimental tests of a rotary active magnetic regenerator prototype. *Int J Refrig* 58: 14-21. doi:https://doi.org/10.1016/j.ijrefrig.2015.05.004.
- ESDU - ENGINEERING SCIENCES DATA UNIT.. 1991. Effectiveness-NTU relationships for the design and performance evaluation of two-stream heat exchangers, ESDU 86018.
- FÄHLER S & PECHARSKY VK. 2018. Caloric effects in ferroic materials. *MRS Bulletin* 43(4): 264-268. doi:10.1557/mrs.2018.66.
- FORTKAMP FP, LANG GB, LOZANO JA & BARBOSA JR. 2020. Design trade-offs for an active magnetic regenerator device. *Appl Therm Eng* 165: 114467.
- GNIELINSKI V. 2013. On heat transfer in tubes. *J Heat Mass Transf* 63: 134-140. doi:https://doi.org/10.1016/j.ijheatmasstransfer.2013.04.015.
- GONÇALVES JM, MELO C & HERMES CJ. 2009. A semi-empirical model for steady-state simulation of household refrigerators. *Appl Therm Eng* 29(8): 1622-1630. doi:https://doi.org/10.1016/j.applthermaleng.2008.07.021.
- GRECO A, APREA C, MAIORINO A & MASSELLI C. 2019. A review of the state of the art of solid-state caloric cooling processes at room-temperature before 2019. *Int J Refrig* 106: 66-88.
- HEIMEL M, BERGER E, POSCH S, STUPNIK A, HOPFGARTNER J & ALMBAUER R. 2016. Transient cycle simulation of domestic appliances and experimental validation. *Int J Refrig* 69: 28-41. doi:10.1016/j.ijrefrig.2016.06.007.
- HERMES CJ & MELO C. 2008. A first-principles simulation model for the start-up and cycling transients of

household refrigerators. *Int J Refrig* 31(8): 1341-1357. doi:<https://doi.org/10.1016/j.ijrefrig.2008.04.003>.

HERMES CJ, MELO C, KNABBEN FT & GONÇALVES JM. 2009. Prediction of the energy consumption of household refrigerators and freezers via steady-state simulation. *Appl Energy* 86(7): 1311-1319. doi:<https://doi.org/10.1016/j.apenergy.2008.10.008>.

HIRANO N, MIYAZAKI Y, BAE S, TAKATA H, KAWANAMI T, XIAO F, OKAMURA T & WADA H. 2014. Development of room temperature magnetic heat pump technologies as a national project in Japan. In: 6th IIR International Conference on Magnetic Refrigeration at Room Temperature, Thermag VI, Victoria, Canada, 7-10 September, 2 p.

HITTINGER M, CHAUDRON JB, ELOUAD L, MULLER C, HAEGEL P & VASILE C. 2016. Impact of the integration work on the performance measurements of the magnetocaloric cooling system and its target refrigerated cabinet. In: 7th IIR International Conference on Magnetic Refrigeration at Room Temperature, Thermag VII, Torino, Italy, 11-14 September, 6 p.

INCROPERA FP, DEWITT DP, BERGMAN TL & LAVINE AS. 2006. *Fundamentals of Heat and Mass Transfer*. J Wiley & Sons, 1024 p.

INTERNATIONAL ELECTRONIC COMMISSION. 2015. *Household Refrigerating Appliances – Characteristics and Test Methods – Part 1: General Requirements*. IEC 62552-1, 114 p.

JACOBS S, AURINGER J, BOEDERA, CHELL J, KOMOROWSKI L, LEONARD J, RUSSEK S & ZIMM C. 2014. The performance of a large-scale rotary magnetic refrigerator. *Int J Refrig* 37: 84-91. doi:<https://doi.org/10.1016/j.ijrefrig.2013.09.025>.

JANSSEN M, DE WIT J & KUIJPERS L. 1992. Cycling losses in domestic appliances: an experimental and theoretical analysis. *Int J Refrig* 15(3): 152-158. doi:[https://doi.org/10.1016/0140-7007\(92\)90005-F](https://doi.org/10.1016/0140-7007(92)90005-F).

JOHRA H, FILONENKO K, HEISELBERG P, VEJE C, DALL'OLIO S, ENGELBRECHT K & BAHL C. 2019. Integration of a magnetocaloric heat pump in an energy flexible residential building. *Renew Energy* 136: 115-126. doi:<https://doi.org/10.1016/j.renene.2018.12.102>.

KLEIN SA. 2018. *Engineering Equation Solver (EES), F-Chart Software, Professional Version 10.448*.

LIONTE S, RISSER M & MULLER C. 2021. A 15kW magnetocaloric proof-of-concept unit: Initial development and first experimental results. *Int J Refrig* 122: 256-265. doi:<https://doi.org/10.1016/j.ijrefrig.2020.09.019>.

MARTINEZ-BALLESTER S, LEÓN-MOYA B, VESSON M, GONZÁLVIZ-MACIÁ J & CORBERÁN JM. 2012. Dynamic Performance Simulation of a Household Refrigerator with a Quasi-Steady Approach. In: *Proc. International Refrigeration and Air Conditioning Conference*, Purdue University, Paper 1256, 8 p.

MASTRULLO R, MAURO A, MENNA L, PALMA A & VANOLI G. 2014. Transient model of a vertical freezer with door openings and defrost effects. *Appl Energy* 121: 38-50. doi:[10.1016/j.apenergy.2014.01.069](https://doi.org/10.1016/j.apenergy.2014.01.069).

MELO C, DA SILVA L & PEREIRA R. 2000. Experimental Evaluation of the Heat Transfer Through the Walls of Household Refrigerators. In: *Proc. International Refrigeration and Air Conditioning Conference*, Purdue University, Paper 502: 353-359.

NAKASHIMA AT, FORTKAMP FP, DE SÁ NM, DOS SANTOS VM, HOFFMANN G, PEIXER GF, DUTRA SL, RIBEIRO MC, LOZANO JA & BARBOSA JR JR. 2021. A magnetic wine cooler prototype. *Int J Refrig* 122: 110-121. doi:<https://doi.org/10.1016/j.ijrefrig.2020.11.015>.

PATANKAR SV. 1980. *Numerical Heat Transfer and Fluid Flow*. Hemisphere Publishing Corporation, 197 p.

PEIXER GF, DUTRA SL, CALOMENO RS, DE SÁ N, LANG G, LOZANO JA & BARBOSA JR JR. 2022. Influence of heat exchanger design on the thermal performance of a domestic wine cooler driven by a magnetic refrigeration system. *An Acad Bras Cienc* 94: e20200563. doi:[10.1590/0001-376520220200563](https://doi.org/10.1590/0001-376520220200563).

PERROTIN T & CLODIC D. 2003. Fin efficiency calculation in enhanced fin-and-tube heat exchangers in dry conditions. In: *Proc. Twentieth International Congress of Refrigeration*, Washington DC, Paper ICRO026, 6 p.

RAZNJEVIC K. 1976. *Handbook of Thermodynamic Tables and Charts*. Hemisphere Publishing Corporation, 392 p.

ROGGE O. 2015. From a prototype to a commercial product. In: *2015 Delft Days on Magnetocalorics*, Nov. 02-03, TU Delft, The Netherlands, 2 p.

SHAH RK & SEKULIĆ DP. 2003. *Fundamentals of Heat Exchanger Design*. New Jersey: J Wiley & Sons, 941 p.

SIM JS & HA JS. 2011. Experimental study of heat transfer characteristics for a refrigerator by using reverse heat loss method. *Int J Heat Mass Transf* 38(5): 572-576. doi:<https://doi.org/10.1016/j.icheatmasstransfer.2011.02.007>.

TAGLIAFICO LA, SCARPA F & TAGLIAFICO G. 2012. A compact dynamic model for household vapor compression refrigerated systems. *Appl Therm Eng* 35: 1-8. doi:[10.1016/j.applthermaleng.2011.08.005](https://doi.org/10.1016/j.applthermaleng.2011.08.005).

TOMC U, KLINAR K, NOSAN S, MAJDIČ F, VALENTINČIČ J, LJUBENKO A, MENCINGER J, DREN D & KITANOVSKI A. 2018. Magnetocaloric wine cooler with rare-earth-free magnet assembly. In: 8th IIR International Conference on Magnetic Refrigeration at Room Temperature, Thermag VIII, Darmstadt, Germany, 16-20 September, 2 p.

TREVIZOLI P & BARBOSA JR J. 2020. Overview on Magnetic Refrigeration. In: Reference Module in Materials Science and Materials Engineering, Elsevier, 12 p. DOI: <https://doi.org/10.1016/B978-0-12-815732-9.00025-5>.

VERSTEEG H & MALALASEKERA W. 2007. An Introduction to Computational Fluid Dynamics – The Finite Volume Method, 2nd ed, Prentice-Hall, 257 p.

WANG CC. 2000. Recent progress on the air-side performance of fin-and-tube heat exchangers. *Int J Heat Exchangers* 1: 49-76.

YU B, LIU M, EGOLF PW & KITANOVSKI A. 2010. A review of magnetic refrigerator and heat pump prototypes built before the year 2010. *Int J Refrig* 33(6): 1029-1060. doi:10.1016/j.ijrefrig.2010.04.002.

ZSEMBINSZKI G, DE GRACIA A, MORENO P, ROVIRA R, ÁNGEL GONZÁLEZ M & CABEZA LF. 2017. A novel numerical methodology for modelling simple vapour compression refrigeration system. *Appl Therm Eng* 115: 188-200. doi:<https://doi.org/10.1016/j.applthermaleng.2016.12.059>.

How to cite

CALOMENO RS, DUTRA SL, SÁ NM, PEIXER GF, LOZANO JA & BARBOSA JR JR. 2022. Temperature pull-down of a retrofitted wine refrigerator cabinet cooled by a caloric system emulator. *An Acad Bras Cienc* 94: e20201510. DOI 10.1590/0001-3765202220201510.

Manuscript received on September 20, 2020; accepted for publication on February 4, 2021

RICARDO S. CALOMENO

<https://orcid.org/0000-0001-7916-2747>

SERGIO L. DUTRA

<https://orcid.org/0000-0002-1933-5797>

NATÁLIA M. DE SÁ

<https://orcid.org/0000-0002-5584-6279>

GUILHERME F. PEIXER

<https://orcid.org/0000-0002-5238-4910>

JAIME A. LOZANO

<https://orcid.org/0000-0003-2682-9952>

JADER R. BARBOSA JR.

<https://orcid.org/0000-0002-8753-6670>

Universidade Federal de Santa Catarina, Departamento de Engenharia Mecânica, POLO - Laboratórios de Pesquisa em Refrigeração e Termofísica, Campus Trindade, 88040-900 Florianópolis, SC, Brazil

Correspondence to: **Jader R. Barbosa Jr.**

E-mail: jrb@polo.ufsc.br

Author contributions

JAL and JRB obtained funding for the research. RSC, GFP, JAL and JRB developed the theoretical formalism. RSC implemented the model and performed the simulations. RSC, SLD, NMS, GFP and JAL conceived, planned and executed the experiments. RSC, SLD, NMS, GFP, JAL and JRB analysed the data. RSC and JRB wrote the manuscript with input from all authors.



APPENDIX

Heat Exchanger 1 (CHEx #1)

Type/material: tube-fin/cooper

Tube length: 11.00 cm

Heat exchanger width: 2.21 cm

Heat exchanger height: 15.2 cm

Tube inner diameter: 6.50 cm

Tube outer diameter: 8.7 cm

Tube pitch: 2.15 cm (longitudinal) / 2.54 cm (transversal)

Number of tubes: 6

Number of fins: 41

Fin thickness: 0.2 mm

Fin width: 2.21 cm

Fin height: 15.20 cm

Heat Exchanger 2 (CHEx #2)

Type/material: tube-fin/cooper

Tube length: 11.00 cm

Heat exchanger width: 4.30 cm

Heat exchanger height: 15.50 cm

Tube inner diameter: 6.50 cm

Tube outer diameter: 7.96 cm

Tube pitch: 2.15 cm (longitudinal) / 2.54 cm (transversal)

Number of tubes: 12

Number of fins: 39

Fin thickness: 0.2 mm

Fin width: 4.30 cm

Fin height: 15.50 cm